RSC Sustainability

ROYAL SOCIETY OF CHEMISTRY

PAPER

View Article Online
View Journal | View Issue

Cite this: *RSC Sustainability*, 2023, **1**, 2277

Co-Al-CO_3 layered double hydroxide: an efficient and regenerable catalyst for glycolysis of polyethylene terephthalate†

Deepthi Thomas, [ab] Rakesh Ranjan[a] and Benny Kattikanal George *[c]

Polyethylene terephthalate (PET) is one among the common polymers we use in our day-to-day lives. Despite its wide range of applications, recycling of PET waste is a serious concern due to its non-biodegradability. This paper deliberates the use of Co-Al-CO_3 layered double hydroxide (LDH) as a catalyst for the glycolysis of PET and the mechanistic aspects of catalysis. Co-Al-CO_3 LDH showed superior properties compared to similar LDH materials. 100% PET conversion and 96% yield for bis hydroxy ethylene terephthalate (BHET) were achieved within a reaction time of 2 hours, at a reaction temperature of 180 °C and with a catalyst concentration of 1%. Glycolysis conditions such as reaction temperature, time, and ethylene glycol (EG)/PET ratio were optimized. The effect of M^{+2}/M^{+3} on BHET yield was studied, and an increase in BHET yield was observed up to a ratio of 3 : 1. The replacement of Co^{2+}, either completely or partially with another M^{2+}, resulted in a significant decrease in BHET yield. The catalysis mechanism of Co-Al-CO_3 LDH was explained by correlating the decarbonation temperature of the carbonate anion with catalytic performance. Magnetically separable CoAl31@Fe_3O_4 was prepared with a BHET yield of 99%. Regeneration was demonstrated up to 4 cycles and a BHET yield of 86% was achieved in the fourth cycle.

Received 31st August 2023
Accepted 15th October 2023

DOI: 10.1039/d3su00304c

rsc.li/rscsus

Sustainability spotlight

Recycling resources are essential for a carbon-neutral society. Especially non-biodegradable polymers such as Polyethylene terephthalate (PET) pose serious environmental concerns of plastic waste accumulation. Though glycolysis is a commercially viable route for PET recycling, the reaction is very sluggish in the absence of a catalyst. This work reports a reusable layered double hydroxide catalyst 'Co-Al-LDH' with a high bishydroxy ethylene terephthalate (BHET) yield of 96%. With the use of our new catalyst, we envisage glycolysis as a closed-loop reaction where along with the feedstock recycling of PET, the catalyst and reactant (ethylene glycol) can be regenerated and reused to realize the "Responsible Consumption and Production" of the Sustainable Development Goals (SDGs).

1. Introduction

Polyethylene terephthalate contributes about 8% of the world's total plastic production and is the fourth most produced polymer after polyethylene, polypropylene, and polyvinyl chloride.[1] Advantages like non-toxicity, transparency, and durability made it widely useful for producing mineral water bottles, soft drink bottles, packaging, fabrics, and films. As the major uses of PET are for disposable items, its recycling should be addressed seriously to reduce solid waste production. The non-biodegradable nature of PET aggravates the environmental pollution issues and currently, PET contributes about 12% by volume of the world's total solid waste production.[2]

Mainly two approaches are used for recycling PET, mechanical recycling and chemical or feedstock recycling. Chemical recycling, where the polymer is chemically depolymerized into commercially valuable monomer/oligomeric molecules, is considered the most sustainable way of recycling.[3–5] Glycolysis is an established method for the chemical recycling of PET, where the PET molecule is depolymerized using ethylene glycol to its monomer bis hydroxy ethylene terephthalate. BHET can be further utilized for PET production or other materials like polyurethanes and acrylate coatings.[3]

PET glycolysis is a slow process in the absence of a catalyst and often results in partially glycolyzed products instead of BHET. Catalysts reported for PET glycolysis can be categorized into metal derivatives,[6–16] ionic liquid (IL) based,[17–19] deep eutectic solvent (DES)[20–24] and organic catalysts.[25–30] Metal-based catalysts include metal salts,[31,32] metal oxides,[8,33–36] metal–

[a]*Analytical and Spectroscopy Division, Vikram Sarabhai Space Centre, Indian Space Research Organization, Thiruvananthapuram 695022, Kerala, India*

[b]*Department of Applied Chemistry, Cochin University of Science and Technology, Cochin 682022, India*

[c]*Analytical, Spectroscopy and Ceramics Group, Vikram Sarabhai Space Centre, Indian Space Research Organization, Thiruvananthapuram 695022, India. E-mail: bkgeorge63@gmail.com*

† Electronic supplementary information (ESI) available. See DOI: https://doi.org/10.1039/d3su00304c

organic frameworks (MOFs),[37] metal nanoparticles,[6,14–16,38] metal oxide doped graphene[11,39], CNTs[40] and layered double hydroxides (LDHs).[41] Ionic liquids have emerged as green catalysts, but they suffer from low BHET yield and difficulty in catalyst regeneration.[17,42,43] Nanocatalysts have received recent attention due to their intrinsic properties, promoting the catalysis process. Sodium and zinc titanate nanotubes,[44,45] ultra-small cobalt nanoparticles,[9] γ-Fe_2O_3/N-doped graphene,[46] boron nitride nanosheets (h-BNNS) decorated with Fe_3O_4 nanoparticles,[7] MnO_2/graphene oxide nanosheets,[11] magnetic Mg-Al-O@Fe_3O_4 microparticles[47] and Fe_3O_4 nanodispersions[15] are some of the nanocatalysts reported for PET glycolysis. 100% BHET yield is reported for (h-BNNS) decorated with Fe_3O_4 nanoparticles at 200 °C in an autoclave when reacted for 5 h.[7] 100% BHET gain was also achieved by γ-Fe_2O_3/N-doped graphene at 190 °C and 1.1 bar pressure.[46] Magnetic Fe_3O_4 nanoparticles prepared by co-precipitation[14] are the latest additions to this group and the authors have reported a BHET yield of 93% at 195 °C for 2 h. High BHET yields are reported for most nanocatalysts, but high reaction temperature and pressure, and complex synthesis methods are drawbacks for most of them.

Cobalt-containing catalysts such as ultra-small cobalt nanoparticles,[9] cobalt oxide from spent lithium-ion batteries,[48] magnetic nanoparticles Co Fe_2O_4,[49] and cobalt-based ionic liquids on graphene support[50] have been reported as promising catalysts for PET glycolysis with up to 95% BHET yield.

Layered double hydroxides (LDHs) are layered materials with M^{2+} and M^{3+} metal hydroxides in the main layers and interlayer spaces containing anionic species.[51] LDH materials are promising entrants in the field of catalysis due to their simple synthesis methods, easily tunable properties, surface hydroxyl groups, presence of basic and Lewis acid sites, variability of intercalating anions, and biocompatibility.[52–54] The major catalytic applications of LDH materials are as the precursor for mixed metal oxide catalysts. LDH materials are catalysts for aldol and Knoevenagel condensations, Michael reactions, and trans-esterification reactions.[55,56] Recently LDH and exfoliated LDH layers gained a lot of scientific attention as photocatalysts for aerobic degradation of pollutants,[57,58] water splitting,[57,59,60] and CO_2 photo-reduction.[61] Though hydrotalcite-derived mixed metal oxides are explored as catalysts for PET glycolysis,[34,47,62] only limited literature is available on the direct use of LDHs as a catalyst for glycolysis. Chen *et al.*[34] studied the catalytic properties of hydrotalcite with different Mg/Al ratios and Mg–Al mixed oxides derived from them for PET glycolysis. A BHET yield of 66.4% was obtained for Mg-Al-CO_3 with an Mg/Al ratio of 3. Eshaq *et al.*[41] presented (Mg–Zn)–Al layered double hydroxide as a regenerable catalyst for PET glycolysis. They could achieve a BHET yield of 75% with 100% PET conversion and the reuse of the catalyst without appreciable loss in efficiency was also reported.

To the best of our knowledge, no reports are available on the utilization of Co-Al-LDH as a transesterification catalyst for PET. This work presents a systematic study on the catalytic activity of Co-Al-LDH for PET glycolysis. Different LDH materials were synthesized by the co-precipitation method and the synthesized materials were characterized and tested for PET glycolysis. Co-Al-LDH which gave the maximum BHET yield was selected for further studies. Glycolysis conditions were optimized and the BHET obtained was characterized by different analytical techniques. The effects of the M^{2+}/M^{3+} ratio and replacement of Co^{2+} with other ions on the BHET yield were also explored.

2. Experimental

2.1 Materials

Co $(NO_3)_2 \cdot 6H_2O$ (Alfa Aesar, 98%), $Al(NO_3)_3 \cdot 9H_2O$ (Alfa Aesar, 98%), $Mg(NO_3)_2 \cdot 6H_2O$, $Ni(NO_3)_2 \cdot 6H_2O$ (Aldrich, 98%), sodium hydroxide pellets (Alfa Aesar, 98%), Na_2CO_3 (Alfa Aesar, 99%) and ethylene glycol (Alfa Aesar, 99%) were used as such. BHET (Sigma Aldrich, >98%) was used after recrystallization. PET cut pieces (dimensions – 1–2 mm) were obtained from waste mineral water bottles. HPLC grade methanol (99.9%, Sigma Aldrich) was used for HPLC analysis of the glycolyzed products.

2.2 Synthesis of LDH materials

2.2.1 Synthesis by co-precipitation. For the preparation of LDH materials M^{2+} and M^{3+}metal nitrates were taken in the required mole ratio and dissolved in 500 ml water. 2 g of NaOH and Na_2CO_3 were dissolved in 50 ml water and added to the metal nitrate solution dropwise with vigorous stirring until the pH reached 12. The mixture was left for 12 hours with constant stirring. After aging, the precipitate is filtered and washed with deionized water until the washings are neutral.

2.2.2 Synthesis of Co-Al31@Fe_3O_4. Co-Al31@Fe_3O_4 was prepared by co-precipitation of cobalt and aluminum nitrates in a suspension of Fe_3O_4 as reported by Koilraj *et al.*[63]

2.3 PET glycolysis[31,41]

1.0 g of PET pieces obtained from mineral water bottles, 0.01 g (1%) LDH, and 10 ml ethylene glycol were refluxed in a 100 ml two-necked round bottom flask at 180° for 2 hours with a stirring rate of 600 rpm. After 2 hours the temperature was decreased to 100 °C and the unreacted PET that remained in the solution was separated. Then, hot water was added to the system and filtered to separate the catalyst. The filtrate was kept at 4 °C for 12 hours to precipitate BHET. Precipitated BHET was washed with water and dried at 80 °C for 12 Hrs. The dried BHET was characterized by FTIR, FTNMR, DSC, and HPLC techniques.

The BHET yield was calculated using HPLC analysis. The products obtained after the glycolysis reaction were filtered to remove the catalyst and insoluble oligomers if any, and the filtrate was made up to 100 ml using HPLC grade methanol. This solution was diluted to a suitable concentration using methanol and injected into the HPLC. The concentration of BHET in the sample was estimated using the calibration graph generated using standard BHET. The BHET yield was calculated as follows:

$$\text{BHET yield}(\%) = \frac{\text{Weight of BHET} \times \text{Mw of PET} \times 100}{\text{Weight of PET} \times \text{Mw of BHET}}$$

where Mw of BHET corresponds to the molecular weight of BHET (254 g mol^{-1}) and Mw of PET is the molecular weight of the PET repeating unit (192 g mol^{-1}).

The PET conversion was calculated using the following equation.

$$\text{PET conversion}(\%) = \frac{W_1 - W_2}{W_1} \times 100$$

where W_1 and W_2 are the initial weight of PET and the weight of unreacted PET, respectively.

2.4 Characterization

FTIR spectra were recorded using a Nicolet iS50 FTIR spectrometer. The IR spectra of LDH materials and BHET were recorded in the region of 400–4000 cm^{-1} by pelletizing with KBr. The IR spectrum of PET was taken using an attenuated total reflectance (ATR) accessory. All spectra were recorded with a resolution of 4 cm^{-1} and 36 scans were accumulated. Scanning electron microscopy (SEM) imaging analysis was carried out using a Carl Zeiss Gemini 500 field emission scanning electron microscope (FESEM) with Bruker detectors. Before analysis samples were given a conductive coating of Au/Pd (80 : 20). The melting point was found using a TA instruments 2920 DSC. The sample was placed on an aluminum pan and then heated from 25 to 250 °C at a rate of 5 °C min^{-1} under a N_2 flow of 10 ml min^{-1}.

^1H and ^{13}C nuclear magnetic resonance (NMR) spectra and ^1H NMR spectra were recorded using a Bruker Avance 400 MHz NMR spectrometer. CDCl3 was used as the solvent. X-ray diffraction (XRD) measurements were carried out using a Bruker D8-Discover X-ray diffractometer operating with a Cu anode (40 KV and 40 mA). A PerkinElmer OPTIMA 4300V was used for elemental analysis by inductively coupled plasma atomic emission spectrometry (ICP-AES). High-pressure liquid chromatography (HPLC) analyses were carried out with a PerkinElmer LC 300 UHPLC using methanol as the eluent at a flow rate of 0.3 ml min^{-1} and a C8-column.

3. Results and discussion

3.1 Characterization of the catalyst

Co-Al-CO_3 LDH with a Co^{2+}/Al^{3+} ratio of 3 : 1 was synthesized by the co-precipitation method and the material is denoted as Co-Al-31 for further reference. Co-Al-31 was characterized by FTIR spectroscopy, XRD, SEM, and ICP-AES. The XRD pattern shows Bragg reflections of basal planes (003) and (006) as shown in Fig. 1. The d_{003} spacing of 7.7 Å is characteristic of an LDH with carbonate as the interlayer anion. The unit cell parameters c and a, calculated from d_{003} and d_{010} values, are 22.98 Å and 3.08 Å, respectively. These values are typical of a hydrotalcite-type crystal structure. The crystallite size calculated using Scherrer's equation is 10 nm. The FTIR spectrum (Fig. S1†) has peaks at 752, 592, and 547 cm^{-1}, which are attributed to the M–OH stretching modes of Co-OH, Co-(OH)-Al, and Al-OH, respectively. Peaks due to the asymmetric stretching of the carbonate interlayer anion are seen in the region 1354–1360 cm^{-1}. A broad

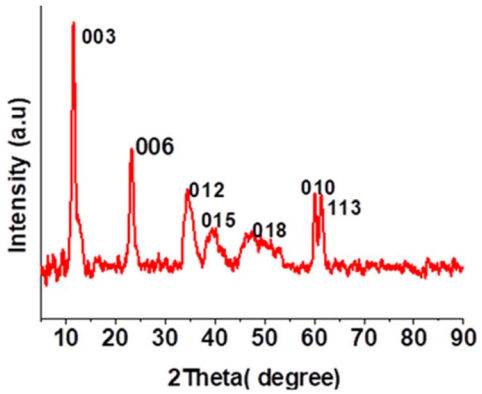

Fig. 1 XRD of Co-Al-31.

peak at 3400 cm^{-1} is assigned to the –OH of the LDH layers and a shoulder around 3000 cm^{-1} is attributed to the –OH stretching of water molecules hydrogen bonded to the intercalated carbonate anion. The surface area of Co-Al-31 evaluated using the BET method is 50.6 m^2 g^{-1}. The surface morphology of Co-Al-31 (Fig. 2) studied using SEM revealed that the material contains nanoplatelets of size <50 nm.

3.2 Catalytic activity of Co-Al-31 in PET glycolysis

PET glycolysis was performed at 180 °C for 2 hours, with 1% catalyst and an EG/PET ratio of 10, and the degradation products were analyzed. BHET crystallized out from glycolysate was characterized by FTIR and NMR spectroscopy (Fig. S2–S4†). The signals at 61.3, 67.0, 166.0, 133.9, and 129.7 ppm in ^{13}C NMR are characteristic of the BHET monomer. The absence of the signal at 63.0 ppm corresponding to the BHET dimer also confirmed the purity of the material. The overlaid FTIR spectra (Fig. S2†) of the PET sample used for glycolysis and the separated glycolysis product confirm that PET is converted to BHET. The purity of the separated BHET was verified by differential scanning calorimetry analysis. A sharp endotherm with peak onset at 109 °C is due to the melting of BHET (Fig. 3). HPLC analysis (Fig. 4) of the glycolysate gave a peak at a retention time

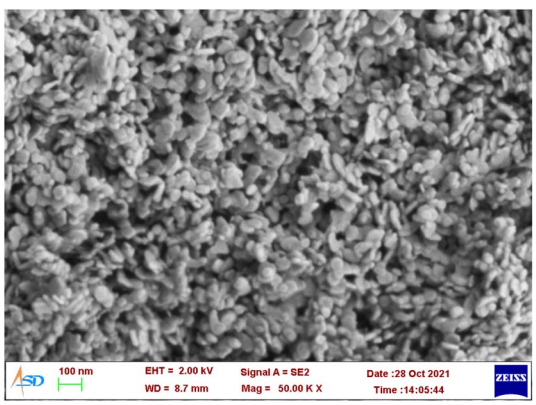

Fig. 2 FESEM image of Co-Al-31.

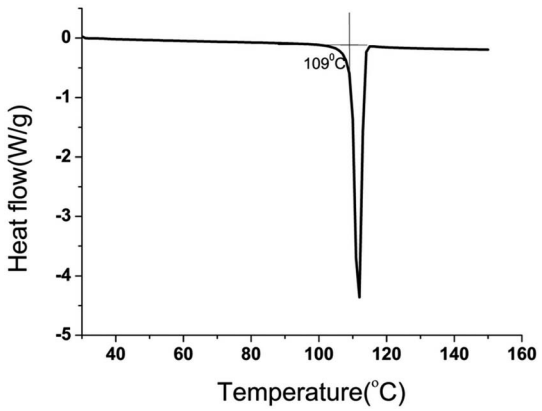

Fig. 3 DSC of BHET from glycolysate.

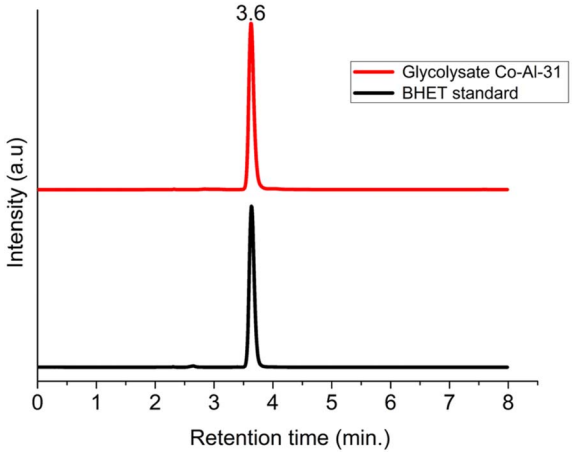

Fig. 4 HPLC of glycolysate and BHET standard.

of 3.5 minutes due to BHET and no dimer peaks are present in the chromatogram.

100% PET conversion and 96% BHET yield were obtained for an EG/PET ratio of 10 and a catalyst concentration of 1% when heated at 180 °C for 2 h. To the best of our knowledge, the BHET yield obtained for CoAl-31 is the highest reported among the hydrotalcite-type materials.

Eshaq *et al.* have reported a 75% yield for (Mg–Zn)–Al LDH[41] and Chen *et al.* have achieved a 66% yield for Mg–Al hydrotalcites.[62]

3.3 Optimization of reaction parameters

The effects of different reaction parameters on BHET yield such as EG/PET ratio, temperature, and reaction time were studied. The EG/PET ratio was optimized by varying the ratio from 5 to 20, keeping the reaction temperature at 180 °C, reaction time at 2 hours, and catalyst concentration at 1%. The BHET yield increased with the increase in the EG/PET ratio and reached a maximum at a ratio of 10 (Fig. 5a). An increase in the ratio above 10 decreased the BHET yield. The PET conversion rate and BHET yield increased with an increase in reaction temperature (Fig. 5b). Increase in the BHET yield was observed up to a temperature of 180 °C and a further increase in temperature could cause only a slight increase in the BHET yield. The reaction time is another factor affecting the BHET yield and the BHET yield increased with the reaction time and reached a maximum value at 2 hours (Fig. 5C). Further increase in the reaction time led to a decrease in the BHET yield. This could be due to the re-polymerization from BHET.[64] It is noteworthy that around 80% yield was obtained within a short time of one hour.

3.4 Effect of the M^{2+}/M^{3+} ratio

Co-Al-LDH materials with $-CO_3^{2-}$ as the interlayer anion were prepared in different M^{2+}/M^{3+} ratios (Fig. S5 and Table S1†) and their catalytic activities for the PET glycolysis reaction were studied. These studies revealed an increase in the BHET yield with an increase in the M^{2+}/M^{3+} ratio (Fig. 6a). An increase in the M^{2+}/M^{3+} ratio from 1 to 3 resulted in a rise in the BHET yield from 76% to 96%. Further increase in the M^{2+}/M^{3+} ratio does not cause any considerable change in the BHET yield.

3.5 Effect of the M^{2+}cation

Cobalt-based catalysts such as cobalt based nanoparticles,[9,49,50] $CoCl_2 \cdot 6H_2O$,[65] Co_3O_4,[48] mechanochemically synthesized $CoFe_2O_4$ (ref. 66) and other mixed metal oxides[48,67] were reported for PET glycolysis. A comparison of the BHET yields of cobalt-based catalysts reported in the literature is given in Table S2.† The BHET yield of Co-Al-31 is in par or even better than those of recently reported catalysts (Table S2†). Comparatively low optimum reaction temperature and simple and energy efficient synthesis are additional advantages for Co-Al-31. The dependence of catalytic activity on the nature of the M^{2+}cation was studied by changing M^{2+} cations while maintaining an M^{2+}/M^{3+} ratio of 3. Mg-Al-LDH, Co-Mg-Al LDH, Ni-Al-LDH, Zn-Al-LDH and Cu-Al-LDH were prepared under similar experimental conditions used for Co-Al-LDH and characterized using XRD and FTIR (S_6). Fig. 6b shows the BHET yields and PET conversion achieved. It is evident from the results that cobalt based LDH has a clear advantage over the rest of the catalysts. The activity is reduced to 88% when Co^{2+} ions are partially replaced by Mg^{2+} ions. Mg-Al-LDH also showed considerable activity as reported by Chen *et al.*[34] Good catalytic efficiencies are reported in the literature for many Zn based catalysts[36,38,67] and Zn-Al-LDH showed a good BHET yield of 88.6% as expected. Drastic decrease in the PET conversion and BHET yield was observed when Ni-Al-LDH and Cu-Al-LDH were employed as catalysts.

3.6 Correlation between the thermal decomposition pattern and catalytic mechanism

The reported mechanism of LDH-catalyzed PET glycolysis involves the synergistic catalysis of Lewis acid and Brønsted basic sites.[35] Metal ions act as Lewis acid sites and –OH and $-CO_3^{2-}$ will act as Brønsted basic sites. According to Liu *et al.*,[68] basic sites in LDHs are the interlayer anions and hydroxyl groups in the layer. For LDH materials with the same interlayer

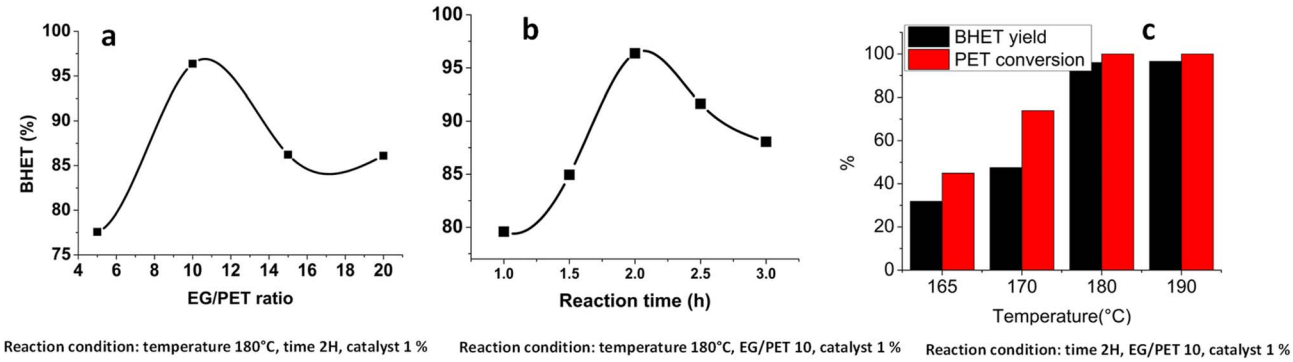

Fig. 5 Effect of the (a) EG/PET ratio, (b) reaction time, and (c) reaction temperature on the BHET yield.

anion, a large difference in catalytic activity was observed upon a change in M^{2+}.

In this scenario, an attempt was made to correlate BHET yield with the bonding strength of the interlayer carbonate. The thermal decomposition path of LDH carbonates involves mainly two mechanisms: loss of water by condensation of –OH (dehydroxylation) and loss of carbon dioxide by the decomposition of interlayer carbonates (decarbonation). The decarbonation temperature of the LDH carbonates can be correlated to the bonding strength of the interlayer carbonate.[69] Carbonates strongly bonded to the cation layer will decarbonate at a higher temperature compared to weakly bonded carbonates. The decarbonation temperatures of the prepared LDH materials were obtained from TG-MS analysis (Fig. 7 and Table 1).

The decarbonation temperatures of the prepared LDH materials are in the order $Cu^{2+} > Mg^{2+} > Ni^{2+} > Zn^{2+} > Co^{2+}$ which matches with the trend in catalytic efficiency. Thus, a correlation can be established between the decarbonation temperature and the catalytic activity of LDH in glycolysis. Cobalt-based LDH materials having a lower decarbonation temperature showed maximum activity. When Co^{2+} is partially replaced by Mg^{2+} ions the peak due to decarbonation splits into two with peaks at 272 °C and 342 °C and the BHET yield decreased to 88%.

Mg-Al-LDH has shown a decarbonation temperature of 372 °C and a BHET yield of 80%. Zn-Al-LDH showed a decarbonation temperature of 337 °C and it also contains a minor amount of strongly bonded carbonates, which decarbonate around 692 °C. This observation justifies the low BHET yield (88.6%) of Zn-Al-LDH compared to Co-Al-LDH. Cu-Al-LDH has strongly bonded carbonates and showed the lowest BHET yield. Ni-Al-LDH is the only mismatch to this trend, where the BHET yield is very low considering its decarbonation temperature of 348 °C. Valente *et al.*[69] also had a similar observation while he was correlating decarbonation temperature with the partial charge on oxygen. SEM analysis of the Ni-Al-LDHs (Fig. S7†) showed aggregation of particles compared to Co-Al-LDH. Even though surface areas are comparable (approx. 50 $m^2\ g^{-1}$) for both materials, access to the interlayer carbonate may be denied by agglomeration. The combined effect of particle aggregation and strong bonding of interlayer carbonates might have led to a reduction in the activity.

Though there are many reports[70,71] on the increase in catalytic activity with the M^{2+}/M^{3+} ratio of hydrotalcite-derived

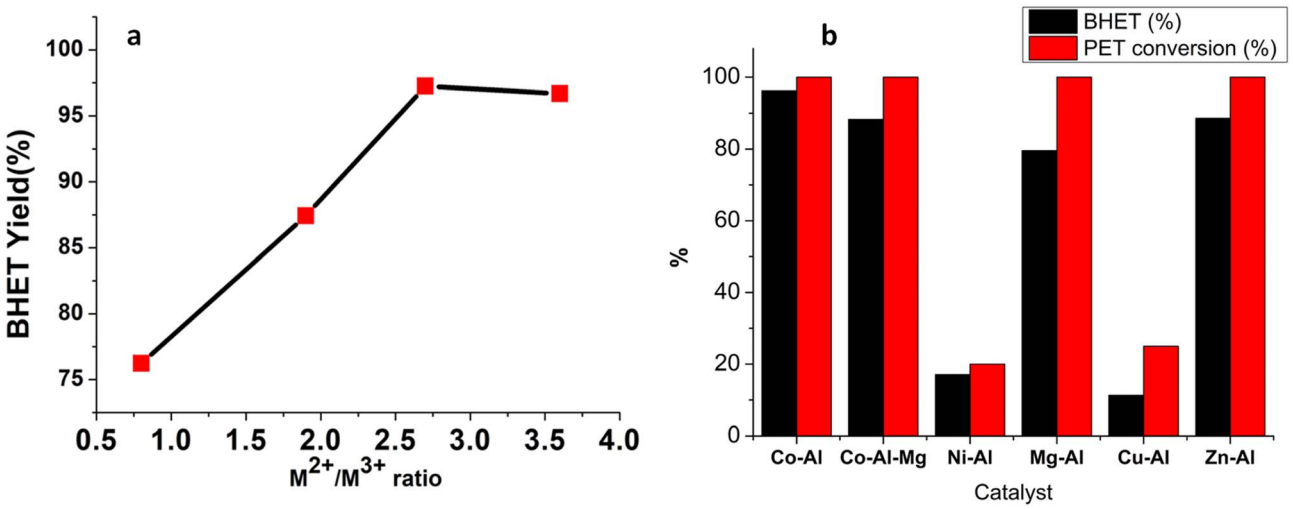

Fig. 6 Effect of the (a) M^{2+}/M^{3+} ratio and (b) M^{2+} ion on the BHET yield.

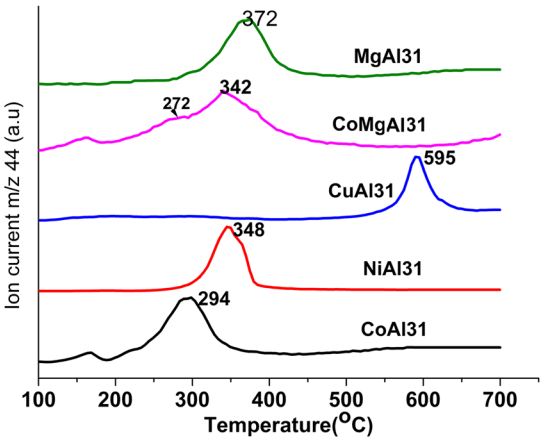

Fig. 7 CO_2 evolution profile of LDHs.

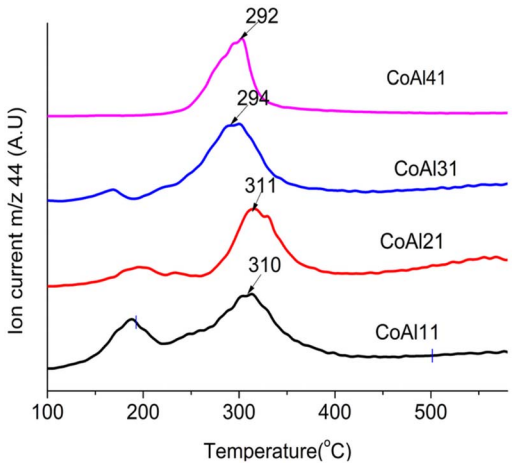

Fig. 8 CO_2 evolution profile of $CoAlCO_3$-LDH of varying Co^{2+}/Al^{3+} ratio.

Table 1 Decarbonation temperature of LDHs

	Catalyst	Peak decarbonation temperature (°C)
1	Co-Al-LDH	294
2	Co-Mg-Al-LDH	342
3	Ni-Al-LDH	348
4	Zn-Al-LDH	337
5	Mg-Al-LDH	372
6	Cu-Al-LDH	595

mixed metal oxides, similar studies are not available for LDH materials. As per previous measurements by Yun[72] and Di Cosimo,[73] an increase of the *c* parameter with increasing Mg/Al molar ratio was observed, which can be correlated to the decreased attractive forces between the brucite-like layers and the interlayer. A decrease in binding energy with an increase in the our study also showed a similar trend for Co-Al-LDH. The M^{2+}/M^{3+} ratio is also proved by modeling studies.[52] As decarbonation temperature is related to the binding strength of the interlayer anion, TG-MS studies are conducted for LDH with varying M^{2+}/M^{3+} ratios from 1 to 4. Fig. 8 shows the decarbonation profile of LDH samples with a change in the Co^{2+}/Al^{3+} ratio. TG-MS studies revealed that as the Co^{2+}/Al^{3+} ratio increases the decarbonation peak shifts towards lower temperature, which in turn increased the catalytic activity. It is interesting to note that, the trend obtained for decarbonation temperature is exactly inverse of that observed for the *c*-parameter (Fig. 9). This result again confirms the correlation of decarbonation temperature with the bonding strength of interlayer anions and cations in the layer.

Glycolysis starts with the attack of deprotonated glycol on the electron-deficient carbonyl carbon of PET. Thus, a good catalyst should make the reaction site electron deficient by withdrawing electrons from the carbonyl bond and facilitating the deprotonation of EG. For LDH-CO_3, the deprotonation of EG will occur by the abstraction of protons either by the interlayer carbonate or by layer hydroxyl. At the same time the interaction of metal cations in the LDH layers will make the carbonyl carbon electron deficient. If interlayer carbonates are strongly bonded to layer cations, the cation's interaction with the carbonyl group of PET will be weak. Adding to this, strongly bonded interlayer anions will be weak deprotonating agents for EG. Thus, an LDH with weakly bonded interlayer anions will be more efficient compared to a strongly bonded one. As discussed earlier, decarbonation temperature can be correlated with the bonding strength of interlayer anions, so LDH-CO_3 with a low decarbonation temperature will be a better catalyst for PET glycolysis. Ethylene glycol can enter the interlayer spaces of LDH, and this enables effective interaction with the interlayer carbonate. A schematic of the mechanism envisaged for catalytic glycolysis is shown in Scheme 1.

3.7 Regeneration of the catalyst

Co-Al-CO_3 catalysts are regenerable and can be reused by filtration. Due to the fine nature of the catalyst direct separation

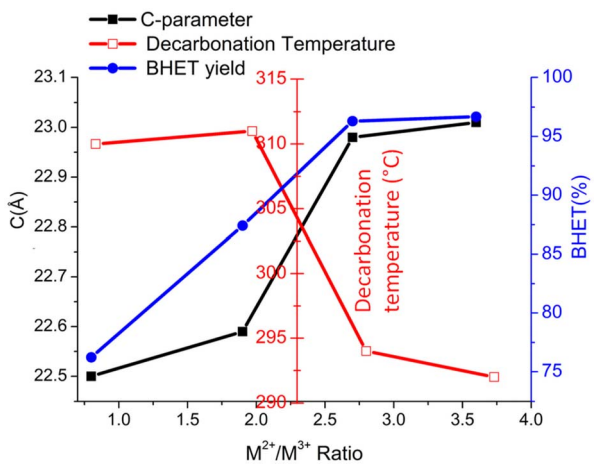

Fig. 9 Variation in the decarbonation temperature and *c*-parameter of $CoAlCO_3$-LDH of varying Co^{2+}/Al^{3+} anion ratio.

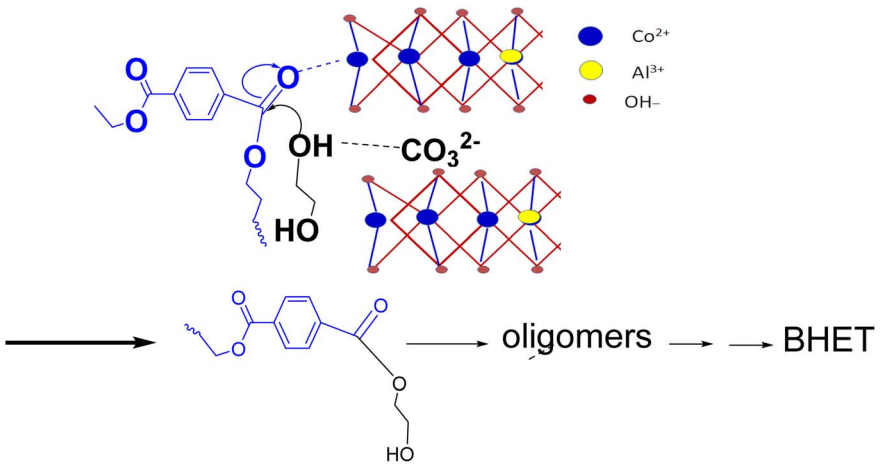

Scheme 1 Schematic of the reaction mechanism.

by filtration creates practical difficulties. To overcome this, magnetically separable LDH catalysts were prepared by coprecipitation of cobalt and aluminum nitrates in a suspension of Fe_3O_4 (ref. 63) keeping a Co^{2+}/Al^{3+} ratio of 3 : 1. The catalyst prepared by this method is named Co-Al31@Fe_3O_4.

Magnetically recoverable catalysts such as paramagnetic ionic liquid-coated SiO_2@Fe_3O_4 nanoparticles,[18] boron nitride

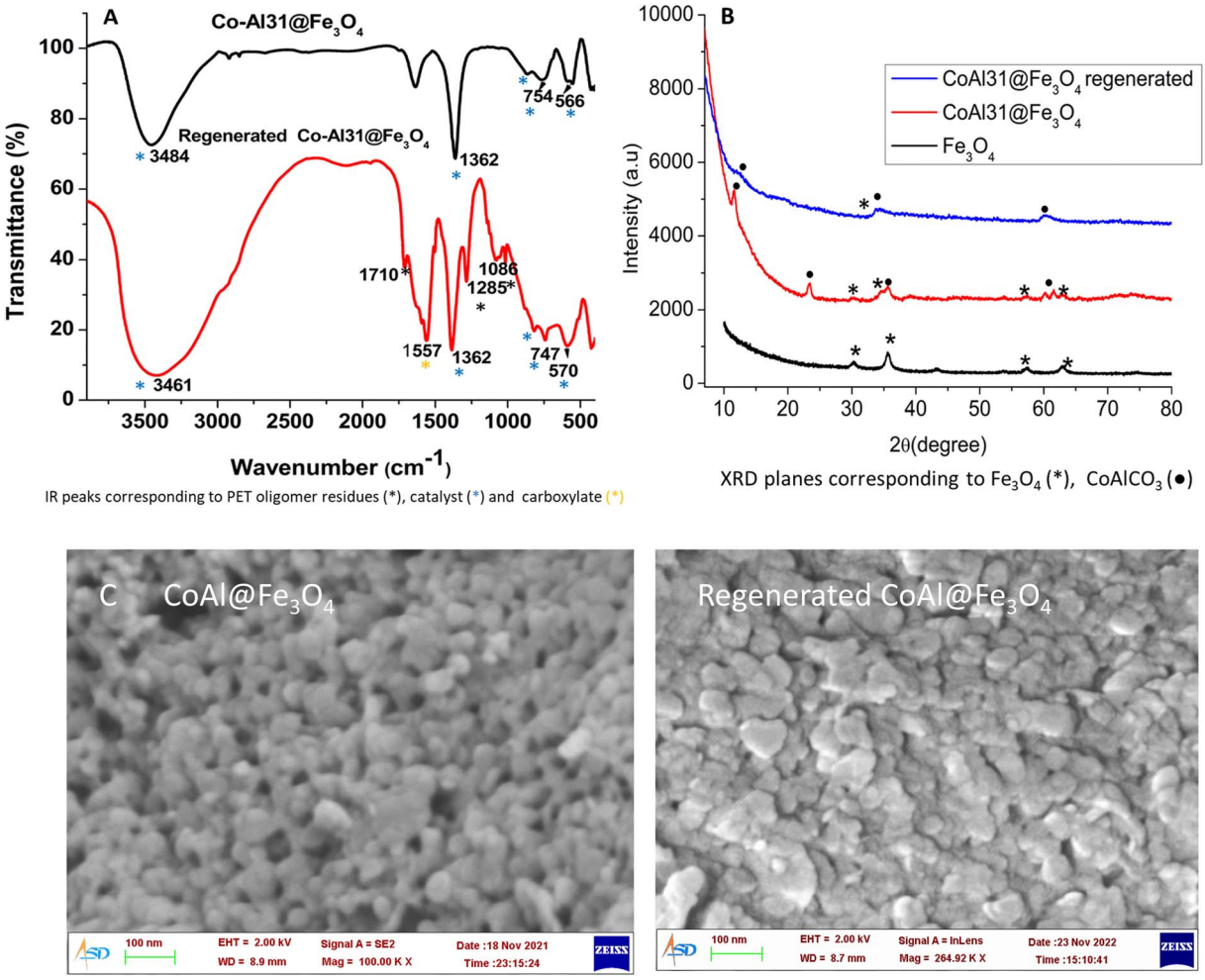

IR peaks corresponding to PET oligomer residues (*), catalyst (*) and carboxylate (*)

XRD planes corresponding to Fe_3O_4 (*), $CoAlCO_3$ (●)

Fig. 10 (A) FTIR spectra, (B) XRD, and (C) FESEM images of fresh and regenerated Co-Al31@Fe_3O_4.

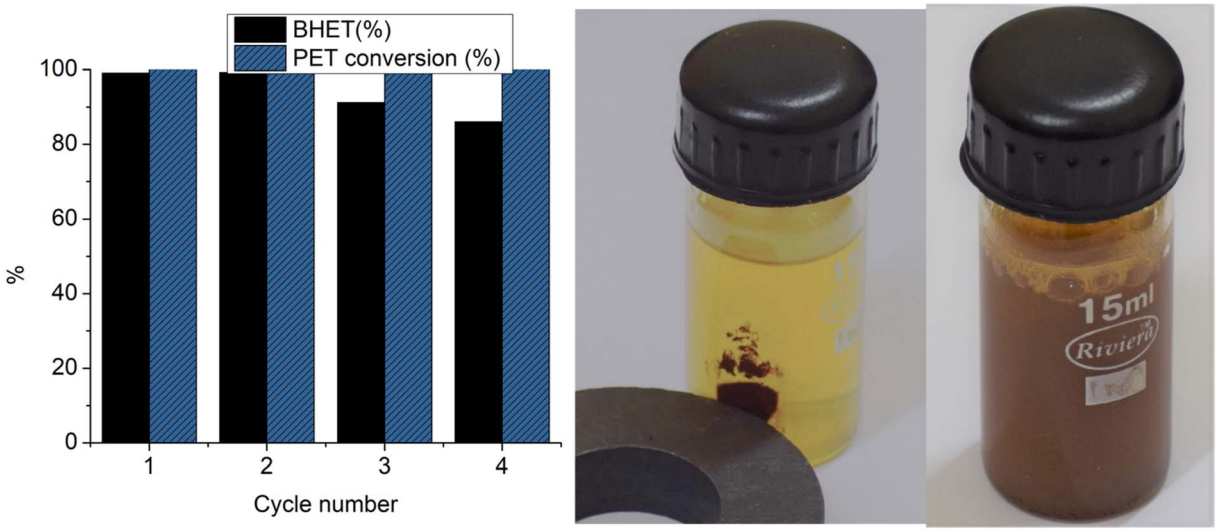

Fig. 11 Regeneration cycles of Co-Al31@Fe_3O_4 and magnetic separation of the catalyst.

nanosheets (h-BNNS) decorated with Fe_3O_4 nanoparticles,[7] superparamagnetic γ-Fe_2O_3 nanoparticles, Fe_3O_4 nanosuspensions,[15] Fe_3O_4 nanoparticles[14] and Mg-Al-O@Fe_3O_4(ref. 47) are reported for PET glycolysis. In addition to easy separation, good catalytic efficiency was also obtained for most of them.

A comparison of the reported magnetically separable catalysts with Co-Al31@Fe_3O_4 is given in Table S3.†

Co-Al31@Fe_3O_4 was characterized by FTIR (Fig. 10A), XRD (Fig. 10B), SEM (Fig. 10C), and ICP analyses (Table S4†). Co-Al31@Fe_3O_4 has 18% iron as per ICP-AES analysis and the FTIR spectrum shows characteristic peaks of carbonate (1362 cm^{-1}), M–OH (566 and 750 cm^{-1}), and –OH (3500 cm^{-1}). The XRD pattern of Co-Al31@Fe_3O_4 has characteristic planes of LDH and Fe_3O_4, but peaks are broadened due to the nanoparticle size of the LDH and ferric oxide.

A BHET yield of 99% was obtained with Co-Al31@Fe_3O_4, which is marginally higher than that obtained for Co-Al-31. As Fe(III) based catalysts are reported to have good catalytic activity, the nano-Fe_3O_4 used for making Co-Al31@Fe_3O_4 was checked for its activity. Fe_3O_4 showed very low PET conversion (2%) and a BHET yield of only 1.6%. The increase in the BHET yield could be attributed to the increase in the surface area when LDH is dispersed on a support.

Four cycles of glycolysis reactions were carried out with Co-Al31@Fe_3O_4. BHET yields and PET conversion achieved in each cycle are depicted in Fig. 11. A good BHET yield of 99% was obtained for the first cycle and 86% for the 4th cycle. Though complete PET conversion was observed up to the 4th cycle, a steady decrease in the BHET yield was observed.

The regenerated catalyst was characterized by FTIR, XRD, and SEM analyses (Fig. 10A). The XRD peaks of the regenerated catalyst are further broadened due to the presence of residual PET oligomers in the catalyst (Fig. 10B). The SEM image of the regenerated catalyst has the same morphology as that of the fresh one (Fig. 10C). The FTIR spectrum shows peaks characteristic of LDH at 1362 cm^{-1} due to interlayer carbonate, 566 and 750 cm^{-1} due to M–OH, and 3500 cm^{-1} due to –OH. A peak at 1712 cm^{-1} is due to residual PET oligomers present in the filtered catalyst. The peak at 1557 cm^{-1} is characteristic of the carboxylate anion. The presence of a carboxylate anion peak in the FTIR spectrum points towards the possible side reaction of ester hydrolysis. The hydrolysis product, terephthalic acid, can bond with the cations to form acid salts. This could be attributed to the reduction in the activity of recycled catalysts after a few cycles.

4. Conclusions

Co-Al-CO_3 layered double hydroxide was reported as a promising catalyst for the recycling of PET by glycolysis. Glycolysis conditions were optimized and a BHET yield of 96% was obtained for CoAl-31 at a comparatively low temperature of 180 °C and reaction time of 2 h. BHET obtained from glycolysis was characterized using various analytical techniques. The catalytic activity decreases when Co^{2+} ions are completely or partially replaced by other M^{2+}. The BHET yield can be correlated to the bonding strength of the interlayer carbonate, which is in turn related to the decarbonation temperature of LDH. Magnetic regeneration of the material was achieved by *in situ* formation of LDH in a suspension of nano-Fe_3O_4. 99% BHET yield and 100% PET conversion were achieved with the catalyst. Four cycles of glycolysis were demonstrated without a decline in PET conversion. However, the BHET yield has gradually decreased to 86% after the fourth cycle. Simple synthesis methods and magnetic regeneration make the catalyst a potential candidate for industrial use in the future.

Author contributions

The manuscript was written through contributions of all authors. All authors have given approval to the final version of the manuscript.

Conflicts of interest

There are no conflicts to declare.

Acknowledgements

The authors thank the Director, VSSC, for permission to publish this work. Motivation and guidance by Dr R Rajeev and analytical support given by colleagues in the Analytical and Spectroscopy Division, VSSC, are gratefully acknowledged.

References

1 I. A. Ignatyev, W. Thielemans and B. Vander Beke, *ChemSusChem*, 2014, **7**, 1579–1593.
2 A. Rahimi and J. M. García, *Nat. Rev. Chem*, 2017, **1**, 1–11.
3 R. Francis, *Recycling of Polymers: Methods, Characterization and Applications*, John Wiley & Sons, 2016.
4 J. Aguado and D. P. Serrano, *Feedstock Recycling of Plastic Wastes*, Royal society of chemistry, 2007.
5 B. Geyer, G. Lorenz and A. Kandelbauer, *eXPRESS Polym. Lett.*, 2016, **10**, 559–586.
6 L. C. S. H. Rezende, J. H. de Oliveira, V. P. M. Zart, M. P. Moisés, G. P. Otto and S. L. Fávaro, *Acta Sci., Technol.*, 2019, **41**, e37303.
7 M. R. Nabid, Y. Bide and M. Jafari, *Polym. Degrad. Stab.*, 2019, **169**, 108962.
8 L. Bartolome, M. Imran, K. G. Lee, A. Sangalang and J. K. Ahn, *Green Chem.*, 2014, **16**, 279–286.
9 F. R. Veregue, C. T. Pereira da Silva, M. P. Moisés, J. G. Meneguin, M. R. r. Guilherme, P. A. Arroyo, S. L. Favaro, E. Radovanovic, E. M. Girotto and A. W. Rinaldi, *ACS Sustain. Chem. Eng.*, 2018, **6**, 12017–12024.
10 Z. Guo, M. Eriksson, H. de la Motte and E. Adolfsson, *J. Cleaner Prod.*, 2021, **283**, 124579.
11 S. B. Jin, J.-M. Jeong, S. G. Son, S. H. Park, K. G. Lee and B. G. Choi, *Mater. Today Commun.*, 2021, **26**, 101857.
12 J. Cao, Y. Lin, W. Jiang, W. Wang, X. Li, T. Zhou, P. Sun, B. Pan, A. Li and Q. Zhang, *ACS Sustain. Chem. Eng.*, 2022, **10**, 5476–5488.
13 S. Shirazimoghaddam, I. Amin, J. A. Faria Albanese and N. R. Shiju, *ACS Eng. Au*, 2023, **3**, 37–44.
14 Y. Jo, E. J. Kim, J. Kim and K. An, *Green Chem.*, 2023, **25**, 8160–8171.
15 Q. Sun, Y.-Y. Zheng, L.-X. Yun, H. Wu, R.-K. Liu, J.-T. Du, Y.-H. Gu, Z.-G. Shen and J.-X. Wang, *ACS Sustain. Chem. Eng.*, 2023, **11**, 7586–7595.
16 L.-X. Yun, Y. Wei, Q. Sun, Y.-T. Li, B. Zhang, H.-T. Zhang, Z.-G. Shen and J.-X. Wang, *Green Chem.*, 2023, **25**, 6901–6913.
17 A. Al-Sabagh, F. Yehia, G. Eshaq and A. ElMetwally, *Ind. Eng. Chem. Res.*, 2015, **54**, 12474–12481.
18 I. Cano, C. Martin, J. A. Fernandes, R. W. Lodge, J. Dupont, F. A. Casado-Carmona, R. Lucena, S. Cardenas, V. Sans and I. de Pedro, *Appl. Catal., B*, 2020, **260**, 118110.
19 M. Mohan, J. D. Keasling, B. A. Simmons and S. Singh, *Green Chem.*, 2022, **24**, 4140–4152.
20 S. Choi and H.-M. Choi, *Fibers Polym.*, 2019, **20**, 752–759.
21 B. Liu, W. Fu, X. Lu, Q. Zhou and S. Zhang, *ACS Sustain. Chem. Eng.*, 2018, **7**, 3292–3300.
22 E. Sert, E. Yılmaz and F. S. Atalay, *J. Polym. Environ.*, 2019, **27**, 2956–2962.
23 Q. Wang, X. Yao, Y. Geng, Q. Zhou, X. Lu and S. Zhang, *Green Chem.*, 2015, **17**, 2473–2479.
24 R. Wang, T. Wang, G. Yu and X. Chen, *Polym. Degrad. Stab.*, 2021, **183**, 109463.
25 B. Liu, X. Lu, Z. Ju, P. Sun, J. Xin, X. Yao, Q. Zhou and S. Zhang, *Ind. Eng. Chem. Res.*, 2018, **57**, 16239–16245.
26 K. R. Delle Chiaie, F. R. McMahon, E. J. Williams, M. J. Price and A. P. Dove, *Polym. Chem.*, 2020, **11**, 1450–1453.
27 Q. Wang, X. Yao, S. Tang, X. Lu, X. Zhang and S. Zhang, *Green Chem.*, 2012, **14**, 2559–2566.
28 L. Wang, G. A. Nelson, J. Toland and J. D. Holbrey, *ACS Sustain. Chem. Eng.*, 2020, **8**, 13362–13368.
29 K. Fukushima, O. Coulembier, J. M. Lecuyer, H. A. Almegren, A. M. Alabdulrahman, F. D. Alsewailem, M. A. Mcneil, P. Dubois, R. M. Waymouth and H. W. Horn, *J. Polym. Sci., Part A: Polym. Chem.*, 2011, **49**, 1273–1281.
30 Z. Wang, Y. Jin, Y. Wang, Z. Tang, S. Wang, G. Xiao and H. Su, *ACS Sustain. Chem. Eng.*, 2022, **10**, 7965–7973.
31 R. López-Fonseca, I. Duque-Ingunza, B. de Rivas, L. Flores-Giraldo and J. I. Gutiérrez-Ortiz, *Chem. Eng. J.*, 2011, **168**, 312–320.
32 S. Javed, D. Ropel and D. Vogt, *Green Chem.*, 2023, **25**, 1442–1452.
33 Y. Zhao, M. Liu, R. Zhao, F. Liu, X. Ge and S. Yu, *Res. Chem. Intermed.*, 2018, **44**, 7711–7729.
34 F. Chen, G. Wang, W. Li and F. Yang, *Ind. Eng. Chem. Res.*, 2013, **52**, 565–571.
35 Y. Lin, D. Yang, C. Meng, C. Si, Q. Zhang, G. Zeng and W. Jiang, *ChemSusChem*, 2023, **16**, e202300154.
36 Y.-W. Chiao, W. Liao, P. A. Krisbiantoro, B.-Y. Yu and K. C.-W. Wu, *Appl. Catal., B*, 2023, **325**, 122302.
37 Q. Suo, J. Zi, Z. Bai and S. Qi, *Catal. Lett.*, 2017, **147**, 240–252.
38 Y. Li, J. Shen, Q. Liu, Y. Zhu, Z. Pang and M. Ge, *J. Environ. Chem. Eng.*, 2023, **11**, 109816.
39 G. Park, L. Bartolome, K. G. Lee, S. J. Lee and T. J. Park, *Nanoscale*, 2012, **4**, 3879–3885.
40 A. Al-Sabagh, F. Yehia, D. R. Harding, G. Eshaq and A. ElMetwally, *Green Chem.*, 2016, **18**, 3997–4003.
41 G. Eshaq and A. ElMetwally, *J. Mol. Liq.*, 2016, **214**, 1–6.
42 A. Al-Sabagh, F. Yehia, A. Eissa, M. Moustafa, G. Eshaq, A. Rabie and A. ElMetwally, *Polym. Degrad. Stab.*, 2014, **110**, 364–377.
43 Q. Wang, Y. Geng, X. Lu and S. Zhang, *ACS Sustain. Chem. Eng.*, 2015, **3**, 340–348.
44 G. R. Lima, W. F. Monteiro, C. M. Scheid, R. A. Ligabue and R. M. C. Santana, *Catal. Lett.*, 2019, **149**, 1415–1426.
45 G. R. Lima, W. F. Monteiro, R. Ligabue and R. M. C. Santana, *Mater. Res.*, 2017, **20**, 588–595.
46 M. R. Nabid, Y. Bide, N. Fereidouni and B. Etemadi, *Polym. Degrad. Stab.*, 2017, **144**, 434–441.
47 Z. Guo, E. Adolfsson and P. L. Tam, *Waste Manage.*, 2021, **126**, 559–566.

48 C. A. Fuentes, M. V. Gallegos, J. R. García, J. Sambeth and M. A. Peluso, *Waste Biomass Valorization*, 2019, 1–11.
49 T. Wang, Y. Zheng, G. Yu and X. Chen, *Eur. Polym. J.*, 2021, **155**, 110590.
50 S. Najafi-Shoa, M. Barikani, M. Ehsani and M. Ghaffari, *Polym. Degrad. Stab.*, 2021, **192**, 109691.
51 V. Rives, *Layered Double Hydroxides: Present and Future*, Nova Publishers, 2001.
52 H. Yan, X.-J. Zhao, Y.-Q. Zhu, M. Wei, D. G. Evans and X. Duan, *The Periodic Table II*, 2019, pp. 89–120.
53 F. Zhang, X. Xiang, F. Li and X. Duan, *Catal. Surv. Asia*, 2008, **12**, 253–265.
54 D. P. Debecker, E. M. Gaigneaux and G. Busca, *Chem. – Eur. J.*, 2009, **15**, 3920–3935.
55 H.-y. Zeng, Z. Feng, X. Deng and Y.-q. Li, *Fuel*, 2008, **87**, 3071–3076.
56 H. Y. Zeng, X. Deng, Y. J. Wang and K. B. Liao, *AIChE J.*, 2009, **55**, 1229–1235.
57 L. Mohapatra and K. Parida, *J. Mater. Chem. A*, 2016, **4**, 10744–10766.
58 L. Wang, Z. Zhu, F. Wang, Y. Qi, W. Zhang and C. Wang, *Chemosphere*, 2021, 130367.
59 M. Shao, M. Wei, D. G. Evans and X. Duan, *Photofunctional Layered Materials*, 2015, pp. 105–136.
60 H. Boumeriame, E. S. Da Silva, A. S. Cherevan, T. Chafik, J. L. Faria and D. Eder, *J. Energy Chem.*, 2021, **64**, 406–431.
61 S. Ali, M. Asif, A. Razzaq and S.-I. In, *Catalysts*, 2020, **10**, 1185–1195.
62 F. Chen, F. Yang, G. Wang and W. Li, *J. Appl. Polym. Sci.*, 2014, 131.
63 P. Koilraj and K. Sasaki, *J. Environ. Chem. Eng.*, 2016, **4**, 984–991.
64 H. Wang, R. Yan, Z. Li, X. Zhang and S. Zhang, *Catal. Commun.*, 2010, **11**, 763–767.
65 R. Esquer and J. J. García, *J. Organomet. Chem.*, 2019, **902**, 120972.
66 P. A. Krisbiantoro, Y.-W. Chiao, W. Liao, J.-P. Sun, D. Tsutsumi, H. Yamamoto, Y. Kamiya and K. C.-W. Wu, *Chem. Eng. J.*, 2022, **450**, 137926.
67 M. Imran, W. A. Al-Masry, A. Mahmood, A. Hassan, S. Haider and S. M. Ramay, *Polym. Degrad. Stab.*, 2013, **98**, 904–915.
68 H.-M. Liu, X.-J. Zhao, Y.-Q. Zhu and H. Yan, *Phys. Chem. Chem. Phys.*, 2020, **22**, 2521–2529.
69 J. S. Valente, F. Figueras, M. Gravelle, P. Kumbhar, J. Lopez and J.-P. Besse, *J. Catal.*, 2000, **189**, 370–381.
70 S. Arhzaf, M. N. Bennani, S. Abouarnadasse, H. Ziyat and O. Qabaqous, *Mediterr. J. Chem.*, 2020, **10**, 625–633.
71 A. Corma, V. Fornes, R. Martin-Aranda and F. Rey, *J. Catal.*, 1992, **134**, 58–65.
72 S. K. Yun and T. J. Pinnavaia, *Chem. Mater.*, 1995, **7**, 348–354.
73 J. Di Cosimo, V. Dıez, M. Xu, E. Iglesia and C. Apesteguıa, *J. Catal.*, 1998, **178**, 499–510.